Submitted to the Astrophysical Journal
Preprint typeset using LaTeX style emulateapj v. 5/2/11

arXiv:1403.5249v1 [astro-ph.HE] 20 Mar 2014

# CONFIRMATION OF A HIGH MAGNETIC FIELD IN GRO J1008−57

Eric C. Bellm[1], Felix Fürst[1], Katja Pottschmidt[2,3], John A. Tomsick[4], Steven E. Boggs[4], Deepto Chakrabarty[5], Finn E. Christensen[6], William W. Craig[4,7], Charles J. Hailey[8], Fiona A. Harrison[1], Daniel Stern[9], Dominic J. Walton[1], Jörn Wilms[10], and William W. Zhang[11]

*Submitted to the Astrophysical Journal*

## ABSTRACT

GRO J1008−57 is a high-mass X-ray binary for which several claims of a cyclotron resonance scattering feature near 80 keV have been reported. We use *NuSTAR*, *Suzaku*, and *Swift* data from its giant outburst of November 2012 to confirm the existence of the 80 keV feature and perform the most sensitive search to date for cyclotron scattering features at lower energies. We find evidence for a $78^{+3}_{-2}$ keV line in the *NuSTAR* and *Suzaku* data at $> 4\sigma$ significance, confirming the detection using *Suzaku* alone by Yamamoto et al. (2014). A search of both the time-integrated and phase-resolved data rules out a fundamental at lower energies with optical depth larger than 5% of the 78 keV line. These results indicate that GRO J1008−57 has a magnetic field of $6.7 \times 10^{12}(1+z)$ G, the highest of known accreting pulsars.

*Subject headings:* pulsars: individual (GRO J100857); stars: neutron; X-rays: binaries

## 1. INTRODUCTION

GRO J1008−57 is a transient high-mass X-ray binary (HMXB) system with a neutron star primary and a Be companion. It was discovered by the Burst and Transient Source Experiment aboard the *Compton Gamma-Ray Observatory* during a 1.4 Crab giant outburst in July 1993 (Stollberg et al. 1993; Wilson et al. 1994). Optical followup identified its Be-type companion and suggested a distance to the source of 5 kpc (Coe et al. 1994).

Like other Be/X-ray binaries (Be/XRBs), GRO J1008−57 exhibits regular outbursts (Type I) due to accretion transfers during periastron passages as well as irregular giant (Type II) outbursts (for a recent review of Be/XRB systems, see Reig 2011). Its Type I outbursts occur predictably at the 249.48 day orbital period (Kühnel et al. 2013; Levine & Corbet 2006). Kühnel et al. (2013) found that the spectra of GRO J1008−57 during Type I outbursts are similarly regular: the continuum spectrum consists of an exponentially cutoff power-law and a low-energy black body component whose properties correlate strongly with source flux.

Accreting pulsars, of which Be/XRBs are a subclass, characteristically exhibit cyclotron resonant scattering features (CRSFs) in the hard X-ray band due to Compton scattering off of electrons with orbits quantized by the $\sim 10^{12}$ G magnetic field of the neutron star. The observed line energy provides a direct probe of the magnetic field strength, with $E_{\rm cyc} = 11.6 B_{12}/(1+z)$ keV, where $B_{12}$ is the magnetic field strength in units of $10^{12}$ G and $z$ is the gravitational redshift at the emission radius (Canuto & Ventura 1977).

Based on *CGRO*/OSSE spectra, Grove et al. (1995) and Shrader et al. (1999) each reported indications for a possible CRSF at ∼88 keV at low significance ($\sim 2\sigma$) for GRO J1008−57. Their data did not provide energy coverage below 50 keV to search for a lower-energy fundamental CRSF at $\sim$ 45 keV. If the 88 keV feature were confirmed as the fundamental, it would imply that GRO J1008−57 has a magnetic field strength near $10^{13}$ G, the highest of any known accreting pulsar[12] (e.g., Caballero & Wilms 2012).

Subsequent modeling of data taken over a broader energy band with *RXTE*, *INTEGRAL*, and *Suzaku* did not reveal a lower-energy fundamental line in the 40–50 keV region (Coe et al. 2007; Kühnel et al. 2013), and detection of the 88 keV CRSF remained marginal. Wang (2013) reported a $\sim 3\sigma$ detection of a CRSF at 74 keV in a 2009 outburst with *INTEGRAL*.

The regular GRO J1008−57 Type I outburst of September 2012 was followed by several months of irregular flaring before the source brightened into a giant outburst in November 2012. The increased flux triggered *MAXI* on November 9 (Nakajima et al. 2012) and *Swift*-BAT on November 13 (Krimm et al. 2012). Peak flux levels reached 1 Crab in the next week, providing an opportunity to obtain high-statistics observations of the system in outburst. *Suzaku* executed a Target-of-Opportunity (ToO) observation on November 20 and reported a de-

[1] Cahill Center for Astronomy and Astrophysics, California Institute of Technology, Pasadena, CA 91125; ebellm@caltech.edu.
[2] Center for Space Science and Technology, University of Maryland Baltimore County, Baltimore, MD 21250, USA
[3] CRESST and NASA Goddard Space Flight Center, Astrophysics Science Division, Code 661, Greenbelt, MD 20771, USA
[4] Space Sciences Laboratory, University of California, Berkeley, CA 94720
[5] Kavli Institute for Astrophysics and Space Research, Massachusetts Institute of Technology, Cambridge, MA 02139
[6] DTU Space - National Space Institute, Technical University of Denmark, Elektrovej 327, 2800 Lyngby, Denmark
[7] Lawrence Livermore National Laboratory, Livermore, CA 94550
[8] Columbia Astrophysics Laboratory, Columbia University, New York, NY 10027
[9] Jet Propulsion Laboratory, California Institute of Technology, Pasadena, CA 91109
[10] Dr. Karl-Remeis-Sternwarte and ECAP, Sternwartstr. 7, 96049 Bamberg, Germany
[11] NASA Goddard Space Flight Center, Greenbelt, MD 20771

[12] La Barbera et al. (2001) reported an extremely broad CRSF centered at 100 keV for LMC X-4, but these measurements were not confirmed by *INTEGRAL* (Tsygankov & Lutovinov 2005).

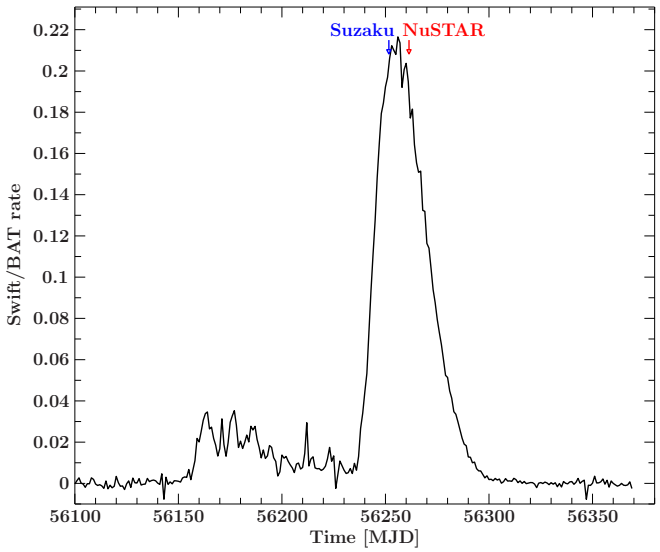


**Figure 1.** *Swift*-BAT light curve of the giant outburst of GRO J1008−57 with the *NuSTAR* and *Suzaku* observation times marked. The BAT count rate is in units of counts $\mathrm{cm}^{-2}\,\mathrm{s}{-1}$.

tection of a cyclotron line at $E_{\mathrm{cyc}}$ =74–80 keV, with the exact energy depending on the continuum modeling (Yamamoto et al. 2013, 2014).

Thanks to its focusing hard X-ray telescopes, *NuSTAR* (Harrison et al. 2013) provides unprecedented sensitivity in the broad 3–79 keV band. *NuSTAR*'s continuous energy coverage removes a major source of systematic errors when fitting broad-band models, while the large effective area and lack of pile-up enables high-statistics time-resolved spectroscopy for bright sources. *NuSTAR* is capable of executing ToO observations within 24 hours of trigger and is thus an ideal instrument with which to study cyclotron lines across a wide range of magnetic field strengths in neutron star binary systems (e.g., Fürst et al. 2013, 2014). *NuSTAR* observed GRO J1008−57 on November 20, shortly after the peak of the outburst (Figure 1).

In this paper we combine *NuSTAR*, *Swift* (Gehrels et al. 2004), and *Suzaku* (Mitsuda et al. 2007) observations of the November 2012 giant outburst in order to obtain the best constraints on the existence of the putative cyclotron line. §2 describes the observations and data reduction. In §3, we perform a series of spectral fits of the *NuSTAR*, *Suzaku*, and *Swift* data. We fit continuum models (§3.1) as well as the previously reported CRSF (§3.2) to the data. Monte Carlo tests confirm the significance of the feature. We perform searches for generic CRSFs at lower energies in both the time-integrated (§3.3) and phase-resolved data (§3.4). We conclude in §4.

## 2. OBSERVATIONS

*NuSTAR* performed a TOO observation of GRO J1008−57 beginning at UTC 2012-11-30 8:41:07 and ending at UTC 2012-11-30 17:31:07. The total on-source observation time was 12.4 ksec after excluding occultation intervals and South Atlantic Anomaly passages.

We processed the data with HEASOFT 6.15 and the *NuSTAR* Data Analysis Software (NuSTARDAS) v. 1.3.0 using CALDB version 20131223. We extracted source counts from circular regions with 4.5 arcmin radius from both *NuSTAR* modules. Because of the brightness of the source, flux from the PSF wings was present over most of the focal plane, preventing extraction of a representative background region. Instead, we scaled the background observed during deep pointings on the Extended *Chandra* Deep Field South region obtained immediately after the GRO J1008−57 observations (e.g., Del Moro et al. 2014). The background was selected from the *NuSTAR* orbital phases matching the GRO J1008−57 observation and was extracted from the same detector region as the source. The background is negligible over most of the *NuSTAR* band; it only reaches 10% of the source count rate at 60 keV, and is 30–60% of the source rate in the 70–78 keV range.

*Swift* obtained a 2.3 ksec snapshot of GRO J1008−57 during the *NuSTAR* observation beginning at UTC 2012-11-30 11:09:25. We reduced the *Swift*-X-Ray Telescope (XRT; Burrows et al. 2005) Windowed Timing mode data using standard procedures in HEASOFT 6.13 and CALDB version 20120830.

*Suzaku* observed GRO J1008−57 earlier in its outburst beginning at UTC 2012-11-20 14:44:31; see Yamamoto et al. (2014) for an independent analysis of these data. The exposure time was 50.4 ksec with the Hard X-ray Detector (HXD; Takahashi et al. 2007). The X-ray Imaging Spectrometer (XIS; Koyama et al. 2007) observed the source in burst mode, resulting in an exposure time of 9.1 ksec.

We reduced data from XIS modules 0, 1, and 3 using standard procedures in HEASOFT 6.13 and CALDB version 20130724. Response files were created using the FTOOL task `xisresp` with the medium option, selecting the default binning. We used extraction regions with 80 arcsec radius and excluded the inner parts of the PSF, roughly following the 5% pile-up contours. Pile-up was estimated using the `pileest` routine, after correcting for residual attitude wobble using `aeattcor2`. We combined the $3 \times 3$ and $5 \times 5$ editing modes where available into one spectrum using `XSELECT`.

We reduced data from the HXD with the standard pipeline using calibration files as published with HXD CALDB 20110913. Spectra were extracted using the tools `hxdpinxbpi` and `hxdgsoxbpi` for the PIN diodes and GSO scintillator, respectively. We obtained the tuned background models from the *Suzaku* website[13], as well as the recommended additional ARF for the GSO.

## 3. SPECTRAL FITTING

We fit the data using the *Interactive Spectral Interpretation System* (ISIS; Houck & Denicola 2000) v1.6.2-19. For all instruments except for the *Suzaku* GSO data (for which the binning scheme was determined by the background modeling), we rebinned the data to $\sim$1/3 of the FWHM of the energy resolution to avoid oversampling the intrinsic detector resolution. We minimized $\chi^2$ in our fits to the data.

The high source flux highlights systematic uncertainties in the response matrices, so we exclude some regions from spectral fits. We fit the *NuSTAR* data in the 5–

[13] `ftp://legacy.gsfc.nasa.gov/suzaku/data/background/pinnxb_ver2.0_tuned/` and `ftp://legacy.gsfc.nasa.gov/suzaku/data/background/gsonxb_ver2.6/`

78 keV range. The *NuSTAR* response falls off sharply beginning around 78 keV, so this upper bound minimizes the effect of response modeling uncertainties on our cyclotron line fits. The *NuSTAR* data showed residual deviations in the 3–5 keV range when fit with data from *Swift* and *Suzaku*, so due to the unusual brightness of the source we omit this region to avoid biasing the fit. We also omit the *NuSTAR* data from 68–70 keV, which is near the tungsten K-edge and has a known response feature which could bias our cyclotron line searches. Similarly, we omit the *Swift* data in the 0.2–1 keV range and above 9 keV due to residual features not seen in the XIS data. We also apply a 3% systematic error per spectral bin. Finally, we fit the *Suzaku* XIS data in the bands suggested by Nowak et al. (2011): 0.8–1.72 keV, 1.88–2.19 keV, and 2.37–7.5 keV. We fit the PIN data in the 20–70 keV band and GRO in the 60–120 keV band.

### 3.1. *Continuum Fitting*

We fit two models frequently used in modeling accreting pulsar spectra to the time-integrated continuum spectra: a powerlaw with a high-energy cutoff, and an `npex` model consisting of two powerlaws with negative and positive spectral indices and an exponential cutoff (Makishima et al. 1999). We also included a Gaussian iron line and a low-energy black body component. For fits including data from *Suzaku* XIS, a second Gaussian component was needed to adequately fit the iron line complex. We used an updated version of the Wilms et al. (2000) absorption model (`tbnew`) as a neutral absorber with `wilm` abundances (Wilms et al. 2000) and `vern` cross-sections (Verner et al. 1996). For the powerlaw with high-energy cutoff, we removed residuals due to the discontinuity at the cutoff energy with a Gaussian absorber tied to the cutoff energy (e.g., Coburn et al. 2002, and references therein). We allowed the normalizations to vary between all instruments being fit.

In contrast to the fits to Type I bursts reported by Kühnel et al. (2013), we found the `npex` model provides a better fit for all combinations of instruments despite having fewer free parameters, so we restrict our attention to this model for further analysis. Yamamoto et al. (2014) similarly found that the `npex` model provided the best fit to the *Suzaku* data from this giant outburst. Table 2 provides the best-fit values for the time-integrated continuum parameters, and Figures 2–5 show the best fits.

The brightness of the source highlights systematic effects in joint fits between multiple instruments, producing poor goodness of fit. Only the *NuSTAR*-only fit has a reasonable goodness of fit, at $\chi^2_\nu = 1.18$ for 536 degrees of freedom. There is substantial disagreement between the instruments below 10 keV (e.g., Figure 5). The *NuSTAR* and *Suzaku* observations are not simultaneous, and so some spectral evolution may have occured between the two epochs. However, there is also disagreement even among the three XIS modules (Figure 4). This disagreement at low energies, driven primarily by XIS1, leads to differences in the best-fit blackbody temperature and power-law indices (Table 2). These discrepancies were also noted in this dataset by Kühnel et al. (2013) and Yamamoto et al. (2014); these authors elected to excise several energy ranges from the XIS backside-illuminated detectors or exclude the data entirely. The fit for the

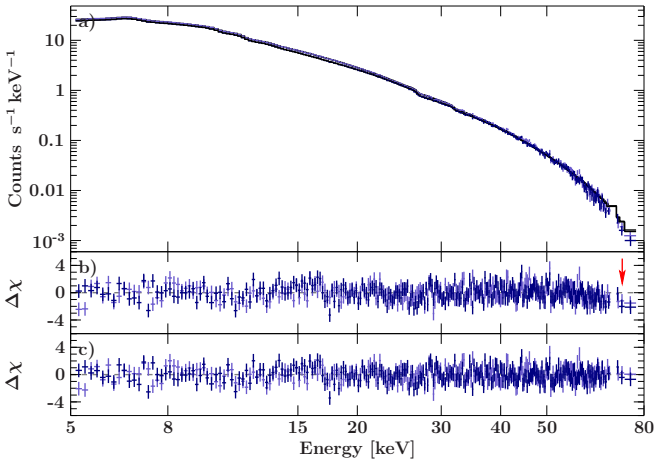


**Figure 2.** Panel a) Count spectrum and `npex` model fit to the *NuSTAR* data. Panel b) Residual plot for the `npex` fit. Panel c) Residual plot for a `npex` fit with `cyclabs` component. An arrow in panel b shows the centroid of the CRSF fit in panel c.

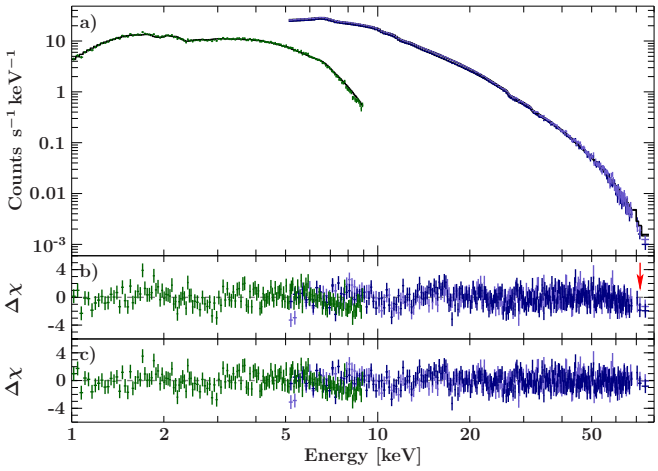


**Figure 3.** Joint *NuSTAR*–*Swift*-XRT fit. *NuSTAR* data are in blue, XRT data are in green. Panels as in Figure 2.

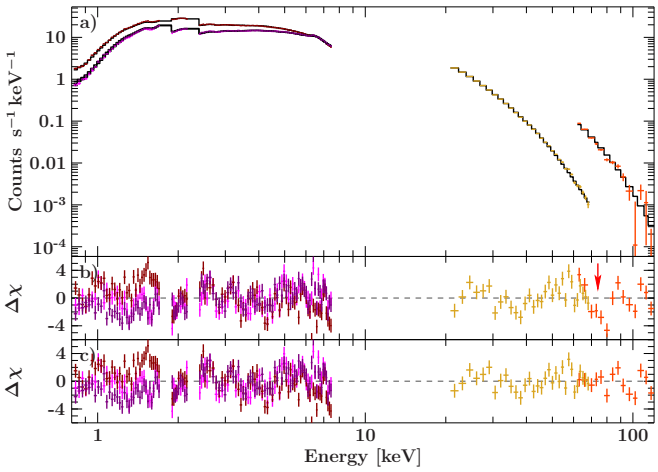


**Figure 4.** *Suzaku*-only fit. XIS data are red, pink, and purple, PIN data are yellow, and GSO data are orange. Panels as in Figure 2.

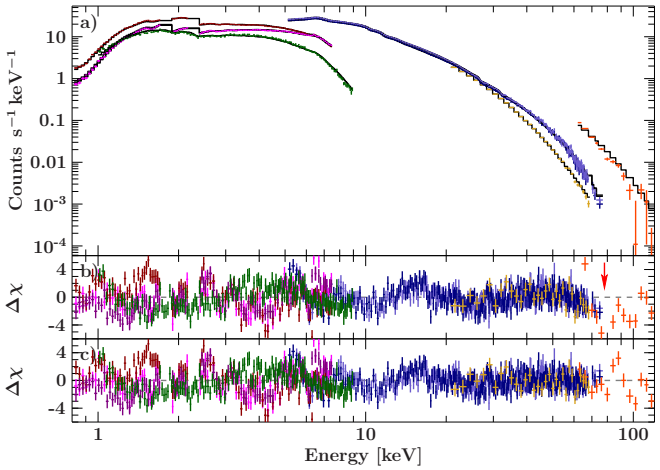


**Figure 5.** Joint *NuSTAR–Swift–Suzaku* fit. Panels as in Figure 2.

blackbody temperature shows multiple minima in the *Suzaku*-only fit, for example, with the $\sim 3$ keV temperature preferred to the 0.4 keV temperature suggested by the joint fit to all instruments. Similarly, our coarser binning and inclusion of all three XIS modules results in better fits to the iron line complex with two broadened Gaussians rather than the narrow 6.4, 6.67, and 7 keV lines fit by Kühnel et al. (2013) and Yamamoto et al. (2014). We are primarily interested in the spectral behavior at high energies, which is well above the folding energy $E_{\rm fold}$ and hence relatively insensitive to these parameters.

### 3.2. *Evidence for a Cyclotron Line*

Next, we fit the data using the above continuum model and a multiplicative cyclotron scattering feature using a pseudo-Lorentzian optical depth profile (the XSPEC `cyclabs` model, Mihara et al. 1990). We initially confined our search to line centers above 50 keV, with fits initialized near the 75 keV value reported by Yamamoto et al. (2013). Table 3 reports the best-fit parameters, while Figures 2–5 compare the residuals to fits without a cyclotron line.

Fits to the *NuSTAR* data alone do not provide strong constraints on the CRSF parameters, as there are degeneracies with the continuum modeling because the cyclotron line lies at the upper edge of the *NuSTAR* bandpass. However, there are clear residuals in the *NuSTAR* data above 70 keV, and *NuSTAR*-only fits are significantly improved by the CRSF. The best-fit *Suzaku* CRSF parameters are a reasonable match to those reported in Yamamoto et al. (2014) given the minor differences in analysis methods.

Combining the *NuSTAR* data with *Suzaku* provides an independent confirmation of the line. In the joint fit, the line centroid moves to 78 keV and the best-fit width is 11 keV, matching the values obtained by Yamamoto et al. (2014) in their `npex` fits including XIS. The GSO cross-normalization changes from 1.19 relative to *NuSTAR* in the `npex` fit to 1.38 in the `npex` with cyclotron feature fit. All other cross-normalization constants remain constant within errors (Table 1). The cyclotron-line fit thus produces correctly the expected agreement between the normalizations of *Suzaku* PIN and GSO.

Both the *NuSTAR* and *Suzaku* data thus independently show evidence for a CRSF in the 70–80 keV range. Because the *NuSTAR* data do not cover the entire CRSF, the joint fit provides the best constraint on the line parameters, but the parameters are sensitive to the *NuSTAR* and *Suzaku*-HXD cross-calibration.

**Table 1**
Best-fit cross-normalization constants relative to *NuSTAR* Module A for the joint *NuSTAR–Swift –Suzaku* fit including a cyclotron line. Errors are 90% C.L.

| Instrument | Normalization |
|---|---|
| *NuSTAR* A | $\equiv 1.0$ |
| *NuSTAR* B | 1.014±0.001 |
| *Swift* XRT | 1.325±0.007 |
| *Suzaku* XIS0 | 1.074±0.003 |
| *Suzaku* XIS1 | 1.095±0.003 |
| *Suzaku* XIS2 | 1.115±0.003 |
| *Suzaku* PIN | 1.380±0.004 |
| *Suzaku* GSO | 1.39±0.04 |

We assessed the significance of the detections using the method of posterior predictive p-values (ppp-values, Protassov et al. 2002). Briefly, we simulate many instances of a model without a `cyclabs` feature by folding the spectral model through instrumental responses; the exposure and binning are matched to the real data, and the data and background are perturbed to account for counting statistics. For each simulated dataset, we then fit the null model and a test model with a `cyclabs` feature. For each simulated realization, we determine $\Delta\chi^2$ between the two models and compare the distribution of $\Delta\chi^2$ values for the simulations to the observed value.

If few of the simulated $\Delta\chi^2$ values are as large as observed in the real data, this provides evidence for the CRSF. Rather than restricting the simulated model parameters to those of the best-fit null model, we use the Cholesky method to draw the simulated parameters from a multivariate Gaussian derived from the covariance matrix obtained in the fit to the null model (Hurkett et al. 2008).

We performed 10,000 simulations of the *NuSTAR* data alone as well as the joint *NuSTAR*, *Swift*, and *Suzaku* data. The line energy was allowed to vary in the 50–100 keV range and the line width between 1 and 30 keV. In all cases, the simulated $\Delta\chi^2$ was less than the value observed in the real data, providing $> 3.9\sigma$ evidence for the existence of the line in each of the two fits. In most of the simulated cases, the best-fit depth of the line is zero, and so the two models are indistinguishable. The largest deviation in $\chi^2$ was 17.0 (21.3) for the combined datasets (*NuSTAR* only), far smaller than the $\Delta\chi^2$ values of 278.5 (62.8) seen in the real data. Based on the difference between the observed and simulated $\Delta\chi^2$ distributions, it is clear that the CRSF detection is much more significant in the joint fit than when using *NuSTAR* alone.

Given the distribution of $\Delta\chi^2$ in these simulations, it would be computationally unfeasible to simulate enough realizations to expect a $\Delta\chi^2$ value near the true value and obtain a true ppp-value significance. We can obtain a simple estimate of the significance (and hence the number of simulations required to obtain that chance deviation) by summing the data and model counts in the $\pm 1\sigma$ energy window around the best-fit 78 keV cyclotron line. Dividing the difference between the `npex` model without the cyclotron line and the data in this region by the statistical error allows us to estimate the

level of chance fluctuation needed. The deviations in the *NuSTAR* data (which do not cover the full cyclotron line) are $1.8\sigma$ and $2.3\sigma$ when the modules are considered independently; the deviation in the GSO data taken alone is $8.0\sigma$. We thus expect the GSO measurement to dominate the fit. (We do not correct for trials over energy because the high-energy line was previously reported in other observations.) If taken at face value, the statistical errors would require more than $8 \times 10^{14}$ simulations to achieve deviations in $\chi^2$ comparable to the observed values.

We considered whether systematic calibration uncertainties could be responsible for the observed feature. While the method of ppp-values provides a robust assessment of line significance (Hurkett et al. 2008), it is sensitive to false positives if systematic errors are present. If a line feature is due to inaccuracy in the instrumental responses or the modeled background, ppp-value tests will confirm its statistical significance but not its physical reality. The calibration of the *NuSTAR* responses in the 70–78 keV range is less certain than at lower energies due to the increasing faintness of astrophysical calibrators. However, measured deviations from a fiducial spectrum of the Crab Nebula are < 15% from 70–78 keV (Madsen et al. 2014, in prep). Similarly, few-percent deviations of the Crab spectrum have been measured in *Suzaku* GSO spectra near 70 keV (Yamada et al. 2011). These effects are not large enough to produce the ∼30% deviation seen here, so we conclude that the feature is both significant and real.

### 3.3. *Search for a Lower-Energy Fundamental Line*

We searched for a cyclotron line at half the energy of the 78 keV line reported in Section 3.2. The *NuSTAR* data enable a more sensitive search than is possible with PIN: The combined *NuSTAR* data have an SNR of 135 per keV at 40 keV in these data, compared to 60 for PIN. (Data from both instruments are strongly source-dominated, given the brightness of the outburst.) No obvious residuals are apparent in the time-integrated *NuSTAR* data near ∼38 keV (Figure 2), consistent with previous non-detections in time-integrated data. Some residual structure is present in the *Suzaku*-PIN data below 40 keV (Figure 4). Using PIN data, Yamamoto et al. (2014) reported a possible fundamental with $E_0 = 36.8^{+1.1}_{-0.7}$ keV, optical depth at line center of $0.06^{+0.08}_{-0.03}$, and width of $11.1^{+7.2}_{-10.2}$ keV in their *Suzaku*-only fit, but concluded it is not statistically significant. A double-cyclotron line *NuSTAR–Suzaku–Swift* joint fit with the fundamental restricted to half of the 90% error limits for the 78 keV does fit a line depth at $39.8^{+0.5}_{-1.2}$ keV. It has depth $1.0^{+0.7}_{-0.2}$ and width $6.0^{+8.4}_{-4.5}$ keV. However, the improvement in $\chi^2$ is modest, only 6.3 for three additional free parameters. Our ppp-value simulations of the higher energy line found 47 out of 10,000 simulations had $\Delta\chi^2$ values larger than this, implying $< 2.9\sigma$ significance. A *NuSTAR*-only fit to a line at this position results in a fundamental with depth consistent with zero. The 90% CL upper limit on the optical depth at 39 keV is 0.04. The possible 39 keV fundamental fit by the *Suzaku* data is thus disfavored by the more sensitive *NuSTAR* data. A broader *NuSTAR* search from 34–40 keV (at half of the line centroid identified by the independent *NuSTAR* and *Suzaku* fits) similarly yielded line depths consistent with zero.

We also performed a generic search for lower-energy lines by stepping a `cyclabs` feature through a 2 keV grid of energies over the 10–60 keV range. We used the *NuSTAR* data only, as in the joint fit the residuals show dips (due to response differences highlighted by the brightness of the source, Figure 5c) not present in the *NuSTAR*-only fit (Figure 2c). For speed, the continuum parameters were frozen in the initial search. Only one trial (at 26 keV) fit a line depth greater than zero, and in this case the best fit line width was 1 keV, at the narrowest limit. The value of $\Delta\chi^2$ is 5.4, less than the largest values obtained by chance coincidence in the Monte Carlo simulations of the 80 keV line, and there is a known response calibration feature at this energy. Over all energies, the largest 90% CL upper limit on the optical depth was 0.09 at 52 keV. Accordingly, we can rule out a lower-energy fundamental with greater depths in the time-integrated data.

### 3.4. *Phase-Resolved Fits*

Because cyclotron line intensities and energies may vary with pulse phase (e.g., Fürst et al. 2013), we split the *NuSTAR* observation into phase bins of roughly constant signal-to-noise ratio and conducted spectral fits on each.

We barycentered the *NuSTAR* event data with `barycorr` using the DE200 solar system reference frame (Standish 1982) and applied a correction for light-travel time across the binary orbit using the ephemeris of Kühnel et al. (2013). Figure 6 shows the *NuSTAR* data folded at the best-fit spin period of 93.57434 sec.

The time-resolved data were well-fit by the `npex` spectral model. We fixed the positive power-law index to 2, consistent with the values obtained in the time-integrated fits. The photon indices show a correlation with intensity (Figure 6), while the folding energy shows a mild secular increase throughout the pulse. No obvious deficits are present in the residuals at lower energies.

We attempted to observe phase evolution of the 80 keV CRSF. Using four phase bins, Yamamoto et al. (2014) found only a slight dependence of the CRSF energy on the pulse data using the *Suzaku* data. We froze the width and depth of the CRSF to the best-fit values from the joint *NuSTAR–Suzaku–Swift* fit but left the energy free to vary. However, the relatively limited *NuSTAR* energy coverage of the line does not permit firm constraints on the line energy.

We also performed a harmonic CRSF fit to the phase-resolved data. We fit for a fundamental line in the 34–47 keV range and froze the ∼80 keV harmonic width and depth to the best-fit time-integrated values. In all epochs, the line depth was consistent with zero, the linewidth unconstrained, and the improvement in $\chi^2 < 2$. The 90% C.L. line depth upper limits were in the range 0.09–0.3.

We repeated the generic grid search for low-energy CRSFs in the time-resolved spectra in case phase-dependent intensity was pushing a fundamental below detectability in the time-integrated fit. As in the time-integrated case, the additional CRSF fit widths pegged at the minimum value of 1 keV, fit depths that were consistent with zero, and/or were associated with the small

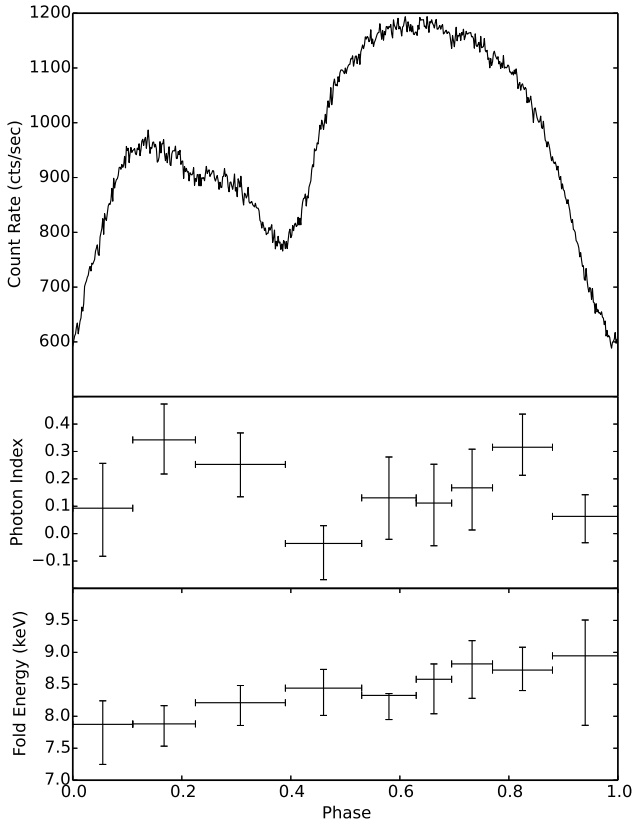


**Figure 6.** *NuSTAR* data (3–79 keV) folded at the 93.57 sec spin period (top panel) and the best-fit phase-resolved `npex` photon indices (middle panel) and folding energies (bottom panel).

known response feature at 26 keV. Over all energies, the largest upper limits on the line depth were 0.2–0.4 and occurred in the 50–60 keV range.

Accordingly, our phase-resolved fits rule out a phase-dependent fundamental CRSF below 70 keV with depth greater than one third of the depth of the 80 keV CRSF.

## 4. DISCUSSION

Observations of the November 2012 giant outburst of GRO J1008−57 with modern instruments provide the best available constraints on the magnetic field strength of this HMXB. Our spectral fits have confirmed that the previously reported CRSF is indeed the fundamental for GRO J1008−57. The best-fit line center for the combined datasets is $78^{+3}_{-2}$ keV. This matches the CRSF reported by Wang (2013) using *INTEGRAL* data but is lower than the 88±5 keV value first reported by Grove et al. (1995). This difference is not highly significant, however. The *Suzaku* data provide a better constraint on the line and higher significance detection because the line centroid is at the upper edge of the *NuSTAR* bandpass, but the *NuSTAR* data provide an independent confirmation of the detection.

The higher sensitivity provided by *NuSTAR* below 79 keV enabled us to perform the most constraining search for a fundamental CRSF at lower energies. Our *NuSTAR* double-cyclotron line fits require the ratio of the optical depths of the fundamental to the harmonic to be less than 5% in the time-integrated data. This is less than the most extreme ratios observed in other accreting pulsars, including Vela X-1 (∼10%; e.g., Fürst et al. 2014) and 4U 0115+634 (≥ 11%, e.g., Müller et al. 2013). In both of those systems, however, phase-resolved fitting reveals intervals of greater fundamental strength. While our phase-resolved limits on the fundamental/harmonic optical depth ratios are less stringent (<11–37%) than the time-integrated constraint, we do not detect a significant fundamental at any phase.

Photon spawning can weaken the strength of the observed fundamental: an electron that scatters into an excited Landau state will release one or more secondary photons with energy comparable to the line energy that may escape to the observer. Calculations suggest this process can replace as much as 75% of the flux in the fundamental CRSF (Schönherr et al. 2007). It thus is difficult to account for the low time-integrated fundamental to harmonic depth ratio we observe with spawning alone. Moreover, spawning is influenced by the hardness of the spectral continuum, with harder spectra producing weaker fundamental lines with more pronounced emission wings (Schönherr et al. 2007). Our nondetection of a low-energy fundamental in the time-resolved fits despite the phase variation in the continuum spectrum (Figure 6) thus argues against such masking.

We therefore conclude that the 78 keV CRSF is likely the fundamental. The inferred magnetic field strength for GRO J1008−57 is $6.7 \times 10^{12}(1+z)$ G, the highest of known accreting pulsars.

This work was supported under NASA Contract No. NNG08FD60C and uses data from the *NuSTAR* mission, a project led by the California Institute of Technology, managed by the Jet Propulsion Laboratory, and funded by the National Aeronautics and Space Administration. We thank the *NuSTAR* Operations team for executing the ToO observation and the Software and Calibration teams for analysis support. This research has used the *NuSTAR* Data Analysis Software (NuSTARDAS) jointly developed by the ASI Science Data Center (ASDC, Italy) and the California Institute of Technology (USA). JW acknowledges partial support from Deutsches Zentrum für Luftund Raumfahrt grant 50 OR 1113.

*Facilities:* NuSTAR, Swift, Suzaku.

## REFERENCES

Burrows, D. N., Hill, J. E., Nousek, J. A., et al. 2005, Space Sci. Rev., 120, 165
Caballero, I., & Wilms, J. 2012, Mem. Soc. Astron. Italiana, 83, 230
Canuto, V., & Ventura, J. 1977, Fund. Cosmic Phys., 2, 203
Coburn, W., Heindl, W. A., Rothschild, R. E., et al. 2002, ApJ, 580, 394
Coe, M. J., Roche, P., Everall, C., et al. 1994, MNRAS, 270, L57
Coe, M. J., Bird, A. J., Hill, A. B., et al. 2007, MNRAS, 378, 1427
Del Moro, A., Mullaney, J. R., Alexander, D. M., et al. 2014, ArXiv e-prints, arXiv:1403.2491 [astro-ph.GA]
Fürst, F., Grefenstette, B. W., Staubert, R., et al. 2013, ApJ, 779, 69
Fürst, F., Pottschmidt, K., Wilms, J., et al. 2014, ApJ, 780, 133
Gehrels, N., Chincarini, G., Giommi, P., et al. 2004, ApJ, 611, 1005
Grove, J. E., Kurfess, J. D., Phlips, B. F., Strickman, M. S., & Ulmer, M. P. 1995, in International Cosmic Ray Conference, Vol. 2, International Cosmic Ray Conference, 1
Harrison, F. A., Craig, W. W., Christensen, F. E., et al. 2013, ApJ, 770, 103

Houck, J. C., & Denicola, L. A. 2000, in ASP Conf. Ser., Vol. 216, Astronomical Data Analysis Software and Systems IX, ed. N. Manset, C. Veillet, & D. Crabtree, 591
Hurkett, C. P., Vaughan, S., Osborne, J. P., et al. 2008, ApJ, 679, 587
Koyama, K., Tsunemi, H., Dotani, T., et al. 2007, PASJ, 59, 23
Krimm, H. A., Barthelmy, S. D., Baumgartner, W., et al. 2012, ATEL, 4573
Kühnel, M., Müller, S., Kreykenbohm, I., et al. 2013, A&A, 555, A95
La Barbera, A., Burderi, L., Di Salvo, T., Iaria, R., & Robba, N. R. 2001, ApJ, 553, 375
Levine, A. M., & Corbet, R. 2006, ATEL, 940
Makishima, K., Mihara, T., Nagase, F., & Tanaka, Y. 1999, ApJ, 525, 978
Mihara, T., Makishima, K., Ohashi, T., Sakao, T., & Tashiro, M. 1990, Nature, 346, 250
Mitsuda, K., Bautz, M., Inoue, H., et al. 2007, PASJ, 59, 1
Müller, S., Ferrigno, C., Kühnel, M., et al. 2013, A&A, 551, A6
Nakajima, M., Mihara, T., Sugizaki, M., et al. 2012, ATEL, 4561
Nowak, M. A., Hanke, M., Trowbridge, S. N., et al. 2011, ApJ, 728, 13
Protassov, R., van Dyk, D. A., Connors, A., Kashyap, V. L., & Siemiginowska, A. 2002, ApJ, 571, 545
Reig, P. 2011, Ap&SS, 332, 1
Schönherr, G., Wilms, J., Kretschmar, P., et al. 2007, A&A, 472, 353
Shrader, C. R., Sutaria, F. K., Singh, K. P., & Macomb, D. J. 1999, ApJ, 512, 920
Standish, Jr., E. M. 1982, A&A, 114, 297
Stollberg, M. T., Finger, M. H., Wilson, R. B., et al. 1993, IAU Circ., 5836, 1
Takahashi, T., Abe, K., Endo, M., et al. 2007, PASJ, 59, 35
Tsygankov, S. S., & Lutovinov, A. A. 2005, Astron. Let., 31, 380
Verner, D. A., Ferland, G. J., Korista, K. T., & Yakovlev, D. G. 1996, ApJ, 465, 487
Wang, W. 2013, ArXiv e-prints, arXiv:1312.6753 [astro-ph.HE], RAA in press
Wilms, J., Allen, A., & McCray, R. 2000, ApJ, 542, 914
Wilson, R. B., Harmon, B. A., Fishman, G. J., et al. 1994, in AIP Conf. Ser., Vol. 308, The Evolution of X-ray Binariese, ed. S. Holt & C. S. Day, 451
Yamada, S., Makishima, K., Nakazawa, K., et al. 2011, PASJ, 63, 645
Yamamoto, T., Mihara, T., Sugizaki, M., et al. 2014, ArXiv e-prints, arXiv:1401.4535 [astro-ph.HE], PASJ in press
—. 2013, ATEL, 4759

**Table 2**
Best-fit time-integrated `npex` parameters for fits with *NuSTAR* (N), *NuSTAR* and *Swift* (NX), *Suzaku* (S), and all instruments (NXS). Errors are 90% C.L. In all fits the positive powerlaw index $\Gamma_2$ was free to vary but converged to the limiting value of 2. Normalization units are photons $\mathrm{keV}^{-1}\,\mathrm{cm}^{-2}\,\mathrm{s}^{-1}$ for the powerlaw components ($A_{1,2}$), photons $\mathrm{cm}^{-2}\,\mathrm{s}^{-1}$ for the Gaussians ($A_{\mathrm{gauss1,2}}$), and $L_{39}/D_{10}^2$ for the black body ($A_{\mathrm{BB}}$), where $L_{39}$ is the source luminosity in units of $10^{39}$ $\mathrm{ergs}^{-1}$ and $D_{10}$ is the distance to the source in units of 10 kpc.

| Parameter | N | NX | S | NXS |
|---|---|---|---|---|
| $N_{\mathrm{H}}$ [$10^{22}$ $\mathrm{cm}^{-2}$] | $1.1^{+1.2}_{-1.1}$ | $1.06 \pm 0.06$ | $1.60 \pm 0.03$ | $1.45 \pm 0.02$ |
| $\Gamma_1$ | $0.15 \pm 0.05$ | $0.27^{+0.06}_{-0.04}$ | $0.94^{+0.02}_{-0.05}$ | $0.30 \pm 0.01$ |
| $A_1$ [$10^{-1}$] | $1.76^{+0.26}_{-0.20}$ | $2.38 \pm 0.15$ | $5.17^{+0.05}_{-0.15}$ | $2.70^{+0.08}_{-0.10}$ |
| $\Gamma_2$ | 2 | 2 | 2 | 2 |
| $A_2$ [$10^{-4}$] | $1.39^{+0.30}_{-0.18}$ | $2.0^{+1.6}_{-0.4}$ | $4.7^{+2.0}_{-0.4}$ | $1.81 \pm 0.07$ |
| $E_{\mathrm{fold}}$ [keV] | $8.44^{+0.14}_{-0.13}$ | $8.34^{+0.38}_{-0.17}$ | $7.47^{+0.16}_{-0.08}$ | $8.17 \pm 0.05$ |
| $E_{0,1}$ [keV] | $6.60 \pm 0.02$ | $6.60 \pm 0.02$ | $6.59 \pm 0.02$ | $6.58 \pm 0.01$ |
| $\sigma_1$ [keV] | $0.29 \pm 0.02$ | $0.30 \pm 0.02$ | $0.28 \pm 0.03$ | $0.27 \pm 0.02$ |
| $A_{\mathrm{gauss,1}}$ [$10^{-3}$] | $6.8 \pm 0.7$ | $7.1 \pm 0.4$ | $9.0^{+1.3}_{-1.4}$ | $6.5 \pm 0.4$ |
| $E_{0,2}$ [keV] | | | $5.4^{+0.2}_{-0.1}$ | $6.0^{+0.2}_{-0.3}$ |
| $\sigma_2$ [keV] | | | $0.07^{+0.03}_{-0.02}$ | $0.19 \pm 0.02$ |
| $A_{\mathrm{gauss,2}}$ [$10^{-3}$] | | | $7.4^{+0.5}_{-0.2}$ | $27^{+7}_{-5}$ |
| $kT$ [keV] | $1.61 \pm 0.03$ | $1.62^{+0.09}_{-0.07}$ | $3.4^{+0.3}_{-0.2}$ | $0.42 \pm 0.02$ |
| $A_{\mathrm{BB}}$ [$10^{-3}$] | $14 \pm 4$ | $8.7^{+1.7}_{-1.4}$ | $79^{+5}_{-7}$ | $3.9^{+0.3}_{-0.2}$ |
| $\chi^2$/dof | 632.6/536 | 881.8/692 | 1134.8/343 | 2424.9/1045 |
| $\chi^2_{\mathrm{red}}$ | 1.18 | 1.27 | 3.31 | 2.32 |

**Table 3**
Best-fit time-integrated `npex` parameters with a cyclotron feature for fits with *Suzaku* (S) and all instruments (NXS). Errors are 90% C.L. Normalizations units are as in Table 2.

| Parameter | S | NXS |
|---|---|---|
| $N_{\mathrm{H}}$ [$10^{22}$ $\mathrm{cm}^{-2}$] | $1.62^{+0.04}_{-0.06}$ | $1.43^{+0.03}_{-0.02}$ |
| $E_{0,\mathrm{cyc}}$ [keV] | $74^{+3}_{-2}$ | $78^{+3}_{-2}$ |
| `cyclabs` width [keV] | $< 5.89$ | $11^{+6}_{-4}$ |
| `cyclabs` depth | $4.2^{+3.8}_{-3.3}$ | $0.81^{+0.15}_{-0.13}$ |
| $\Gamma_1$ | $1.03^{+0.12}_{-0.13}$ | $0.29^{+0.03}_{-0.02}$ |
| $A_1$ [$10^{-1}$] | $5.24^{+0.23}_{-0.29}$ | $2.54^{+0.13}_{-0.17}$ |
| $\Gamma_2$ | $1.10^{+0.04}_{-0.20}$ | 2 |
| $A_2$ [$10^{-4}$] | $52.479^{+0.005}_{-7.573}$ | $1.40^{+0.29}_{-0.19}$ |
| $E_{\mathrm{fold}}$ [keV] | $8.9 \pm 1.0$ | $8.55^{+0.31}_{-0.14}$ |
| $E_{0,1}$ [keV] | $6.589^{+0.002}_{-0.010}$ | $6.58^{+0.01}_{-1.44}$ |
| $\sigma_1$ [keV] | $0.29 \pm 0.03$ | $0.27 \pm 0.02$ |
| $A_{\mathrm{gauss,1}}$ [$10^{-3}$] | $9.3^{+1.3}_{-1.2}$ | $6.5 \pm 0.4$ |
| $E_{0,2}$ [keV] | $5.36^{+0.17}_{-0.10}$ | $5.6^{+0.4}_{-0.5}$ |
| $\sigma_2$ [keV] | $0.63^{+0.25}_{-0.14}$ | $2.07^{+0.32}_{-0.27}$ |
| $A_{\mathrm{gauss,2}}$ [$10^{-3}$] | $5.7^{+0.8}_{-1.9}$ | $34^{+16}_{-9}$ |
| $kT$ [keV] | $2.90^{+0.99}_{-0.26}$ | $0.45 \pm 0.02$ |
| $A_{\mathrm{BB}}$ [$10^{-3}$] | $43^{+31}_{-20}$ | $4.2^{+0.5}_{-0.4}$ |
| $\chi^2$/dof | 1070.7/340 | 2266.0/1042 |
| $\chi^2_{\mathrm{red}}$ | 3.15 | 2.17 |